REPORT DOCUMENTATION PAGE

Form Approved
OMB No. 0704-0188

1. REPORT DATE *(DD-MM-YYYY)*	2. REPORT TYPE	3. DATES COVERED *(From - To)*.
15/08/2003	FINAL TECHNICAL REPORT	15/05/1999 - 15/05/2003

4. TITLE AND SUBTITLE
THE MECHANISMS OF CREEP RESISTANCE OF ADVANCED CERAMIC EUTECTICS: EXPERIMENTS AND MODELING

5a. CONTRACT NUMBER

5b. GRANT NUMBER
F49620-99-1-0276

5c. PROGRAM ELEMENT NUMBER

6. AUTHOR(S)
ARGON, ALI S.
PROFESSOR OF MECHANICAL ENGINEERING

5d. PROJECT NUMBER

5e. TASK NUMBER

5f. WORK UNIT NUMBER

7. PERFORMING ORGANIZATION NAME(S) AND ADDRESS(ES)
MASSACHUSETTS INSTITUTE OF TECHNOLOGY
MECHANICAL ENGINEERING DEPT.
ROOM 1-306
77 MASSACHUSETTS AVENUE
CAMBRIDGE, MA 02139

8. PERFORMING ORGANIZATION REPORT NUMBER

9. SPONSORING / MONITORING AGENCY NAME(S) AND ADDRESS(ES)
AIR FORCE OFFICE OF SCIENTIFIC RESEARCH
DIV. MECHANICS OF MATERIALS & DEVICES, DR. BYUNG-LIP LEE, PROGRAM MANAGER
4015 WILSON BLVD.
AFOSR/NA, ROOM 713
ARLINGTON, VA 22203-1954

11. SPONSOR/MONITOR'S REPORT NUMBER(S)

12. DISTRIBUTION / AVAILABILITY STATEMENT
APPROVED FOR PUBLIC RELEASE, DISTRIBUTION UNLIMITED, AUGUST 2003

13. SUPPLEMENTARY NOTES
NONE

14. ABSTRACT
The creep resistance of the directionally solidified ceramic eutectics of alumina/cubic-zirconia was studied experimentally in the 1200-1520 C, and 100-275 Mpa stress range, with associated TEM and SEM microscopy, as a generic example of ceramic eutectics. Additional computer simulations were done both at the atomic level and by FEM methods to study: a) the core structure of pyramidal edge dislocations in alumina that can only climb but not glide; and b) the stress distribution in the alumina component during creep. A creep model based on diffusional climb of pyramidal system edge dislocations was in very good agreement with the measured creep rates. The model predicts that the creep resistance of the eutectics should be superior to that of pure sapphire fiber in the above temperature range, and must be considered as potential candidates for high temperature structural applications. Exploitation of their full potential in high temperature composites, however, requires extensive engineering materials development.

15. SUBJECT TERMS
Ceramic eutectics; creep resistance; creep models; atomistic simulations of dislocation cores

16. SECURITY CLASSIFICATION OF:			17. LIMITATION OF ABSTRACT	18. NUMBER OF PAGES	19a. NAME OF RESPONSIBLE PERSON
a. REPORT	b. ABSTRACT	c. THIS PAGE			Prof. Ali S. ARGON
unclassified	unclassified	unclassified	NONE	41	19b. TELEPHONE NUMBER *(Include area code)* (617) 253-2217

Final Technical Report on AFOSR Grant F49620-99-1-0276 THE MECHANISMS OF CREEP RESISTANCE OF ADVANCED DIRECTIONALLY SOLIDIFIED EUTECTICS: EXPERIMENTS AND MODELLING

A. S. Argon, PI
Mechanical Engineering Department
Massachusetts Institute of Technology, Cambridge, MA 02139

Table of Contents

Executive Summary

In the quest for development of structural materials with high temperature capability well above 1000°C in primary structural applications many systems have been under consideration. Of these, among ceramic systems, the directionally solidified (DS) eutectic ceramics have demonstrated interesting potential for use in the 1200-1500° range as competitors to sapphire fiber. A system among these eutectics that has such potential but also is relatively simple in composition and morphology is the DS eutectic of Al_2O_3/c-ZrO_2(Y_2O_3).

In the as-solidified form this eutectic combines a topologically continuous majority phase of Al_2O_3 at a volume fraction of c.a. 0.67 with a nearly perfect texture of [0001] parallel to the growth axis that encapsulates a minority phase of cubic ZrO_2 in a submicron fiber or platelet morphology. The low temperature fracture toughness of this eutectic, at a level of c.a. 5MPa $m^{1/2}$ is considered adequate. The behavior of primary importance of this eutectic for structural applications is its creep resistance in the 1200-1500° range within which the morphological stability against coarsening is acceptable. It is the creep resistance of this eutectic that has been under study in this AFOSR-supported research program.

Based on detailed morphological characterization of the eutectic and on some associated computer simulations of dislocation cores as well as FEM studies of the internal stress distributions among phase components under stress, the creep experiments in the range of 1200-1520°C at stress levels up to 300MPa resulted in a creep model that is in very good agreement with experimental findings. The creep model is based on the response of the topologically continuous Al_2O_3 component. It proposes that creep in the Al_2O_3 component results entirely from the diffusion controlled climb of pyramidal edge dislocations which are forced to thread through the sub-micron c-ZrO_2 domains acting as dispersoids. The theory which agrees well with the experimental measurements of steady state creep in the 1200-1520°C range predicts that in this range the eutectics have better creep resistance than pure sapphire of "c" axis orientation, provided that the morphology does not coarsen. This latter, possibly adverse, behavior needs further study.

The exploitation of the very good creep resistance of these eutectics in directionally solidified fiber form will need substantial additional engineering development before material components can be made ready for structural application. Much earlier developments on monazite coatings to prevent surface degradation of eutectic fibers in composites should make such engineering materials systems developments more readily possible.

The research at the Massachusetts Institute of Technology was aided importantly by the collaboration of A. Sayir of the NASA John Glenn Research Center who supplied all the DS eutectics and also contributed to the interpretation of the creep results. Other financial assistance came from the Mechanical Engineering Department at M.I.T. in some equipment acquisitions

and from a NATO Fellowship to a visiting scientist.

Persons involved in the research at M.I.T. included: (Appendix A)

A. S. Argon, PI (15/05/1999 - 15/05/2003)
C. T. Bodur, Visiting Scientist (01/09/2002 - 28/02/2003)
J. Chang, Graduate Student (01/02/2003 - 28/02/2003)
J. Yi, Graduate Student (15/05/1999 - 15/05/2003)

For publications please see Appendix B.

1 Introduction

To reach beyond the capabilities of the present set of high temperature superalloys and some intermetallic compounds that have service limitations at around 1000°C, it is necessary to consider other compounds such as oxides, carbides, borides, etc. to attain service temperatures in the 1400-1600°C range[1]. While these are all intrinsically brittle materials, having low temperature brittleness problems, their high temperature performance is largely governed by their creep resistance and fracture resistance. It is creep resistance that was of principal concern in the completed research program.

For some time, single crystal sapphire fiber with [0001] axis orientation has been considered as an ideal material for high temperature application [2]. In that orientation with its principal basal and prismatic systems unstressed, sapphire single crystal fibers have remarkable creep resistance in the 1400-1600 °C temperature range where only the pyramidal slip system is stressed. Early experiments of Firestone and Heuer [3] on [0001] axis-oriented-sapphire in the 1600-1800°C range produced evidence that such sapphire crystals creep entirely by the climb of the $1/3< \bar{1}101 >$ pyramidal edge dislocations, with no slip line or stereo-TEM evidence of glide of such dislocations on any of the possible pyramidal planes available. That such dislocations are entirely sessile in glide has now been established in very recent MD simulations of the core structures of these dislocations in the present program, and is presented in Section 4.2 [4, 5]. The stress dependence of the creep rates of sapphire crystals of [0001] orientation and their governing activation energy being of oxygen ion diffusion in Al_2O_3 have all been consistent with a pure climb mode of creep [3]. This is extremely rare in the creep of metals, with the only similar occurrence having been reported by Edelin and Pourier [6] in similarly oriented Mg crystals.

While oriented sapphire single crystal fibers have advantageous characteristies and have been considered with diffusion barrier coatings as reinforcing elements in polycrystalline Al_2O_3 matrixes for composite applications [7, 8], the practice has been costly and lacked flexibility. As an alternative to sapphire-fiber-reinforced ceramic composites, a series of directionally solidified advanced ceramic eutectics, consisting largely of an Al_2O_3 component together with compatible stable oxides of ZrO_2 or YAG combine many of the advantages of sapphire fiber with morphological stability at elevated temperatures in the 1500°C range and relative ease of production. Of these the Al_2O_3, ZrO_2 system eutectic, with additional 4.2 mol% Y_2O_3 modification to create cubic ZrO_2, has demonstrated many attractive characteristics [9]. This system was chosen for detailed study in the present research program.

2 Experimental Details

2.1 Material and characterization

The eutectics of Al_2O_3/c-$ZrO_2(Y_2O_3)$[1] have all been produced by the Laser Heated Float Zone (LHFZ) method at the NASA John Glenn Research Center in the facilities of our principal collaborator A. Sayir [9]. Source rods were prepared using 99.999% pure polycrystalline Al_2O_3 powder (CERAC/pure, Ceralox Corp., Tucson, AZ 08676), and 99.999% pure ZrO_2 and Y_2O_3 powders (Alfa Aesar). These powders were blended in acetone for 70 hours. The slurry was dried, mixed again and formed into cylindrical rods using cold isostatic pressing. These rods were then sintered at 1500°C in air for 4 hours. A LHFZ process was used to produce the directional solidification of rods as described previously [2]. The rods were re-used as source rods to produce final samples. The objective of the second solidification was to minimize the entrapment of gases at the liquid solid interface. The directional solidification (DS) rate was at 2mm/min for both processes. The final DS rods had cross-sectional dimensions roughly in the range of 1-1.5 mm diameter changing from rod to rod but showed only small thickness variations along their 20-22 cm length in any one rod. They were composed of 67% Al_2O_3 and 33% c-ZrO_2 by volume. Random sectioning of the rods always showed a certain residual component of $Y_3Al_5O_{12}$ (YAG) at levels that were considered to be insignificant. More significant however was an unavoidable level of porosity along the center line of many samples, often with substantial pore dimensions to constitute super-critical flaws for fracture. These pores always had smooth surfaces indicating they resulted from inadequate wetting during melting and solidification of the initial charge. In a few instances they resulted in fracture during loading of the creep experiments where they were given no further attention other than characterization of the pore sizes and shapes as a feed-back to improve the production process. TEM specimens made from randomly spaced axial and transverse sections were used for electron diffraction to check orientation of components. These, as well as a limited number of X-ray pole figure determinations obtained from surfaces of axial and transverse section of the bars demonstrated that the Al_2O_3 topologically continuous phase had a growth texture of [0001] within 2-3° parallel to the specimen axis [10, 11]. Wherever prominent three-fold symmetrical colony structures of c-ZrO_2 were observable on transverse sections, there were notable angular differences between the symmetry axes of these colonies indicating the presence of small angle tilt boundaries in the Al_2O_3, (often in the range of 10°) with tilt axes parallel to the growth axis. Since such tilt boundaries would not be stressed in samples under tension parallel to the bar axis, they were not considered to be of any importance in the creep behavior.

The c-ZrO_2 phase, in turn, exhibited various morphological shapes ranging from aligned fibers or platelets in either well organized colonies or in less well ordered forms, usually had

[1] About 4.2 mol% of Y_2O_3 is required to form cubic zirconia. This was the case with all the eutectics in the present study. Therefore, hereafter the zirconia is referred to only as c-ZrO_2

one narrow dimension in the 0.2μm range, and was always fully encapsulated in the Al_2O_3 phase with high quality nearly coherent interfaces [13], also verified in the present work with several direct-lattice-imaging TEM observations [23]. The eutectic had fairly reproducible and reasonably attractive levels of fracture toughness [12].

Corresponding determination of the texture of the c-ZrO_2 phase, largely based on electron diffraction information, indicated that this phase had primarily a $< 112 >$ growth texture with fiber symmetry, incorporating random rotations about this axis[1] Figure 1 shows a typical morphology of the Al_2O_3/c-ZrO_2 eutectic. The sketch of Fig. 2 shows pictorially the mutual orientational association of the two component phases.

The DS eutectics contained significant levels of residual stress at room temperature, resulting from thermal misfit between the component phases. The Al_2O_3 was in a state of uniaxial tension parallel to the axis, at a level of 1.0 GPa while the c-ZrO_2 was in some form of multiaxial compression, roughly at the same level [10]. Such residual stresses that decrease in level at elevated temperatures were rapidly relaxed on the onset of steady creep flow.

2.2 Creep equipment and creep strain measurement

The creep experiments were carried out in tension inside a Centorr vacuum chamber containing a specially designed hot zone of 5cm diameter and 5cm length made up of a split cylindrical configuration of a 1mm thick *Ta* sheet with alternating up-and-down slits to increase the path length of the heating element. The hot zone was surrounded by a series of *Mo* radiation shields. The long specimens threaded through the hot zone and were gripped at their ends by specially produced stainless steel friction grips, clamping down on the ends of the specimens through annealed soft nickel sheets to avoid high local contact forces on the rods that could have resulted in fracture. Two relatively massive water cooled OFHC *Cu* plates were placed between the two exits of the hot zone and the specimen grips to assure that the gripping conditions were not to exceed about 200°C to avoid slippage in the grips. Figure 3 shows a schematic layout of the interior of the high temperature high vacuum creep chamber.

An optical grade sapphire window permitted viewing the hot specimen through a narrow axial slit in the heating elements to permit direct measurements of the specimen temperature by means of a two-wave-length pyrometer (from Omega Vanzetti, Sharon, MA.), providing emissivity-independent measurements. In addition to a control thermocouple inside the hot zone, another thermocouple placed close to the specimen without touching it, was used to actually record the steady temperature in the thermal cavity. The temperature measured by this second thermocouple and that measured by the pyrometer on the specimen usually agreed quite well. The hot zone temperature was automatically controlled by the PID control system of the Centorr equipment.

[1]Textures such as $< 111 >$ have also been reported by other investigators.

Since the steady state creep extensions of the specimens under stress were generally quite small, to eliminate random flexures and motions of the massive creep frame from influencing the measurements, the displacements of the two ends of the load train immediately outside the vacuum chamber were simultaneously measured by sets of four LVDTs at both the top and bottom ends of the Centorr chamber. The differences between these two measurements then corresponded to the extension of the specimen. Since the temperature of the specimen inside the hot zone was higher by 1200-1300°C above the portions of the sample outside the hot zone, the gauge length was taken as the axial extent of the hot zone. Even under ideal conditions the total creep strain was never too uniquely determinable. To overcome this difficulty all creep strains at steady state were always measured incrementally at a given temperature under two different applied stresses and often as loading and unloading cycles. This practice of relative measurements of creep strain did not only give more reliable determinations of the strain rates at the two different levels of stress but also demonstrated the nearly complete absence of transients in such incremental changes in steady state creep. A typical response of this type is shown in Fig. 4 for creep at 1520°C at stress levels of 150MPa and 200MPa. The accuracy of strain measurement was around 1.4×10^{-5}.

2.3 Fracture toughness experiments

Fracture toughness of the eutectics was measured by the well known technique of determining the extent of cracking from the corners of Vickers hardness indentations, but by utilizing a more exact technique of determining the open crack contours at the surfaces as described by Haubensack and Argon [14]. The fracture toughness was also estimated from the size and shape of pores in the as-grown eutectics when they gave rise to premature fracture. Some estimates were also made from the measured toughness profiles of fracture surfaces.

2.4 Computational methodologies

Two separate computational studies were carried out in the program. In the one carried out on the dislocation core structures in sapphire at the atomic level, the MOLDY MD programs were used to calculate core structures of edge dislocations on basal planes and pyramidal planes of Al_2O_3. In the FEM computations of distributions of stresses among the two different components of Al_2O_3 and c-ZrO_2 during creep, the commercial ABAQUS code was used.

3 Experimental Results

3.1 Creep experiments

3.1.1 Transient effects

Upon initial application of stress to a virgin specimen a strain transient was always observed. One such transient recorded for an experiment at 1200°C under a stress of 300 MPa is shown in Fig. 5. The characteristic time constant of the transient decreased with increasing temperature, e.g. from c.a. 3.4×10^3sec at 1200°C to 200 sec at 1400°C. The usual explanation of the transient to be due to initial work hardening in the creeping components prior to establishment of a steady state by recovery processes, familiar in creep of homogeneous metals, was discounted here since no prominent transients were found following stress increases at steady state creep. The most likely cause of the initial transient was the rapid stress relaxation in the coarse c-ZrO_2 component by creep since for the measured texture of that component there is an abundance of the $< 110 > \{100\}$ principal slip systems that are well oriented for slip, and the creep resistance of c-ZrO_2 in this temperature range is known to be poor [15]. In more ideal morphologies, as presented by Sayir and Farmer [2] and Argon, et al. [16], the coarse fraction of the c-ZrO_2 is located on colony borders. In the usual less ideal morphologies where fibrillar c-ZrO_2 is still aggregated but does not form well structured colonies the coarse fraction was found to be less regularly distributed (see Fig. 1). An upper bound manifestation of the poor creep resistance of c-ZrO_2 can be assessed from a Finite Element (FEM) study that will be presented in Section 4.1. There it was found that for the complete relaxation of the deviatoric stresses in the entire c-ZrO_2 phase the volume average deviatoric stresses as well as mean normal stresses in the Al_2O_3, increase roughly by 25-30% which would result in an increment of additional elastic strain in the sample of about 6×10^{-4}. This level is illustrated in Fig. 5 by the horizontal line. The actual amount of stress relaxation in the c-ZrO_2, however, is difficult to determine since a substantial fraction of this component has phase dimensions in the range of 0.2-0.4μm and is likely to be dislocation-free and incapable of plastically deforming as we discuss in Section 5.0. These, and the difficulties in determining the absolute measures of strain derived from the hot zone portions of the samples requires us to de-emphasize this portion of the creep response.

3.1.2 Steady state creep

As already mentioned in Section 2.2 the main information on steady state creep was obtained from incremental experiments of sudden stress increases and decreases at constant temperature as shown in the typical case of Fig. 4 of creep response. A simple check of the magnitude of the instantaneous stretches or contractions for stress increases or decreases, utilizing the appropriate information on the temperature dependent Young's modulus of Al_2O_3 [17] gave in all cases that the recorded jumps were all about a factor of 2 larger than what could be

expected from the sample in the hot zone. Since this was well within the additional flexures and relaxations in the load train the recorded strain rates were considered to be reliable.

After the final configuration of the hot zone discussed in Section 2.2 was completed, 11 determinations of steady state creep rate were made, all together at 3 temperatures of 1200, 1400, 1520°C and at stress levels ranging from 150MPa to 275MPa, derived from incremental experiments similar to those in Fig. 4. These measurements are listed in Table 1 and are plotted in Fig. 6 together with the creep rates at 1400°C due to Sayir and Farmer [2], also quoted in [16][1]. The stress exponents of the creep rates at 1400°C and 1520°C, shown in Fig. 6, are 4.16 and 5.38 and are lower than that of Sayir at 6.00. As we will discuss in the creep model in Section 5.1, these exponents are relatively high and need to be explained, as we will do later in Section 5.2.

Table 1 contains also sufficient information for the determination of the activation energy of the governing creep process. The plot of the creep rates at a stress of 200MPa for three temperatures of 1200°C, 1400°C and 1520°C in Fig. 7 gives an activation energy of Q = 71.1 kcal/mol for the rate controlling process in steady state creep which we consider to be due to oxygen ion diffusion that is known to be the slowest diffusing species in Al_2O_3. This value is to be compared with 105 kcal/mol for temperatures above 1400°C and 26 kcal/mol for temperatures below 1400°C for the same process measured by Oishi and Kingery [18] in pure polycrystalline Al_2O_3. The somewhat lower magnitude of the measured activation energy for oxygen ion diffusion is attributed to the likelihood that a significant fraction of the diffusion current must have been along the the incoherent interfaces.

3.2 Fracture toughness measurements

As mentioned in Section 2.3, the fracture toughness was estimated by the open crack contours at the Vickers indentation corners. Fig 8 shows the Vickers indentation and the open crack extending from one of the corners. According to Haubensack and Argon [14], the K_{IC} can be estimated from

$$K_{IC} = \frac{(COD)E}{\mathbf{F}(r/a)r^{1/2}} \tag{1}$$

where $\mathbf{F}(r/a)$ is a non-dimensional characteristic crack-shape factor dependent on the geometry and the mode of loading, a is the crack length, and E is the Young's modulus. The estimated values of K_{IC} of eutectic Al_2O_3/c-ZrO_2 ranged from 2.0 $MPam^{1/2}$ to 5.0 $MPam^{1/2}$.

The fracture toughness can also be estimated from the size and shape of pores in the as-grown eutectic and surface flaws when they lead to premature fracture. In Fig 9, an internal pore and a surface flaw are identified. The estimated fracture toughness is around 1.0 $MPam^{1/2}$.

[1]The higher creep rates and the larger stress exponents in these early investigations are most likely a result of not reaching steady state but still being in a late stage of transient behavior.

The crack deflection by the morphology can be a very effective way in toughening. By measuring the fracture surface profile, the energy release rate can be estimated. In Fig 10 the AFM surface profile characterization of a fractograph is shown. It suggests that the critical energy release rate G_{IC0} is around 1.0 J/m^2, which is reasonable.

4 Computational Results

4.1 Distribution of stress in the Al_2O_3/c-ZrO_2 eutectics in creep

A very important way in which creep in the eutectics differs from creep in single crystal sapphire is that in the former the stresses are distributed in a complex manner. In addition to residual stresses arising from the different thermal expansions of the two components, the applied stresses result in complex internal local stress distributions due to different elastic properties of the Al_2O_3 and the c-ZrO_2 component phases. Thus, to develop some necessary understanding of this phenomenon on a broad basis; a linear-elastic FEM analysis was carried out in a 2-D plane strain setting of the eutectic in the ordered regions shown in Fig. 1. Here the c-ZrO_2 domains in 2-D are idealized as elliptical cylinders occupying a volume fraction of 0.33 as depicted in Fig 11. The chosen representative computational volume (RVE) is indicated in this figure. We have considered the c-ZrO_2 to be always fully relaxed of all shear stresses but with an unrelaxed appropriate bulk modulus of 83GPa. This is accomplished operationally in the FEM code for purely elastic behavior by choosing the Young's modulus of the c-ZrO_2 artifically as 0.05MPa and the Poisson's ratio as 0.4999999. All other chosen material constants are listed in Table 2. The broader analysis was considered for several aspect ratios a/b of ellipsoidal rods of c-ZrO_2 as 1,3,4 and 5. Of these results we present here only the distributions for $a/b = 3.0$ as most representative. All analyses were limited to the elastic range. In this FEM framework we considered several process simulations: a) an applied tensile stress σ_z alone; b) cooling the morphology from a stress-free condition at 1875°C down to 1400°C to determine residual stresses at 1400° and; c) cooling as in (b) plus an applied tensile stress of $\sigma_z = 300$MPa. Of these, we discuss here only the case of the internal stress distribution under an applied stress $\sigma_z = 300$MPa, and the result of a cooling history, from 1875°C (Since behavior is linear-elastic, results for all other applied stress levels can be determined by re-scaling).

In Fig. 12a we show the distribution of the Mises deviatoric stresses for the case of $\sigma_z =$ 300MPa and T=1400°C, in both the Al_2O_3 and c-ZrO_2 regions. As expected, the states of stress inside the ellipsoidal regions of the c-ZrO_2 are close to constant. Figure 12b gives the more important distribution of the climb stress σ_1, parallel to the pyramidal dislocation Burgers vector at an angle of $\phi = 57.7^o$ as shown in Fig. 17. The volume-average level of this important climb producing stress was found to be $\sigma_1 = 216.3$MPa which gives the factor $q = \sigma_1/\sigma_z$ to be 0.721. This value appears surprisingly low in view of the assumed complete relaxation of the deviatoric stresses in the c-ZrO_2, until it is recognized that the c-ZrO_2 still supports fully a

mean normal stress which limits the stress enhancement in the Al_2O_3 component. The factor q enters in an important way into the creep model of the eutectics as described in Section 5.2.

Figure 13a and 13b show the corresponding results for internal deviatoric (von Mises) stresses and mean normal stresses at 1400°C, resulting from a cooling history from 1875°C to 1400°C. Examination of Figs. 13a and 13b shows that the thermal misfit in the Al_2O_3 at 1400°C are in the range of substantial fractions of one GPa, and clearly consistent with the reported residual stresses at room temperature referred to in Section 2.1.

4.2 Simulations of the core structures of edge dislocations in Al_2O_3

As is expanded further in the creep model presented in Section 5.1 the creep resistance of the eutectics are governed by that of the topologically continuous Al_2O_3 component which has a remarkably tight growth texture of [0001] parallel to the growth axis of the eutectic rods. This renders the best glide systems in the base plane and even the prismatic system inoperative. Thus, for geometrical reasons extension of the Al_2O_3 in the [0001] direction by glide or climb can only be possible through the motion of the pyramidal dislocations. According to general consensus glide deformation on the pyramidal dislocations is too difficult to happen and has never been reported, leaving climb of such dislocations as the only realistic possibility. To establish the basis of the impossibility of glide on the pyramidal system a molecular dynamics (MD) simulation was undertaken of the core structure of edge dislocations $1/3 < \bar{1}101 >$ on this slip system using the established MOLDY [26] code. For comparison purposes the core structure of the basal dislocations $1/3 < 2\bar{1}\bar{1}0 >$ was also simulated. The full details of the simulation results which are beyond the scope of this final report have been presented in a comprehensive communication [5] and will not given here. Here only the most important findings are presented.

Figure 14 shows the cation sub-lattice of Al_2O_3 which establishes the principal dislocation Burgers vectors based on the periodicity of the Al cation holes. The three principal slip systems: in the base plane; in the prismatic system and finally in the pyramidal system are clearly identified. The simulations of the base plane dislocations and the pyramidal dislocations required selection of two separate simulation cells shown in Fig. 15 which gives the crystallographic symmetry of the idealized Al_2O_3 lattice as viewed from the "c" direction. In the figure the large open circles show the hexagonal packing of the Oxygen anions in the base planes whereas the small solid black circles and the small open circles show the location of the Al cations and cation holes respectively, on an interstitial plane immediately above the Oxygen plane.

The rectangle ABCD gives the geometry of the base of the simulation cell chosen to simulate the cores of the $1/3 < 2\bar{1}\bar{1}0 >$ basal dislocation, while the rectangle A'ACC' gives the geometry of the base of the simulation cell chosen for simulation of the cores of the $1/3 < \bar{1}101 >$ pyramidal dislocation. In both cases periodic boundary conditions were used to obtain valid simulations of edge dislocation cores, unaffected by surface conditions. To obtain realistic

conditions with rapid convergence of the MD energy relaxations real atom coordinates for the ion lattices were used which differ substantially from the ideal coordinates presented initially by Kronberg [27]. In both simulations to avoid unwanted long range lattice curvatures edge dislocation dipoles were introduced into the simulation cells according to a rigid prescription discussed elsewhere [5].

The principal finding related to the immobility of the pyramidal dislocation is shown in Fig. 16a and 16b which views the Al_2O_3 lattice from the $[11\bar{2}0]$ direction (refer to Fig. 14). Figure 16a shows the unrelaxed core of the initial configuration of the $1/3 < \bar{1}101 >$ pyramidal dislocation located in the $(1\bar{1}02)$ planes made up entirely of cation holes in the cation sublattice. The sketch on the right side of the figure delineates the two extra ion half planes of the dislocation. The final relaxed configuration of the core after minimization of system energy by the MOLDY program is shown in Fig. 16b. The figure indicates that the form of energy minimization that occurs and affects the core structure splits the core into two fractional edge dislocations lying on parallel cation planes on either side of the initially more favorable plane of cation holes, being displaced to planes with both high level covalent and ionic bonding as delineated in the sketch on the right side of the figure. Thus, while the core energy is distinctly reduced the two partial edge dislocations are rendered sessile as a detailed, so-called, gamma surface topography of the potential shear resistance across these planes demonstrate.

The corresponding simulation of the core structure of the base plane edge dislocation $1/3 < 2\bar{1}\bar{1}0 >$ which is not presented here exhibits a very similar splitting of the core structure of the dislocation as in the case of the pyramidal dislocation. In this case, however, since each base plane between adjacent close packed anion planes is identical to all other planes no reduction of mobility results from the core rearrangement.

Thus, in summary, the MD simulations have clearly demonstrated that the pyramidal dislocation can not glide but that their climb motion should be relatively unimpaired.

5 The Creep Model

5.1 Basic assumptions

The fact that the c-ZrO_2 of considerably lower creep resistance is encapsulated everywhere by the topologically continuous Al_2O_3 with a very tight growth texture of [0001] along the axes of the DS eutectic rods indicates that steady state creep must be controlled by the Al_2O_3 phase, once any limited compliance increment due to the stress relaxation in c-ZrO_2 is complete. This suggests that the overall creep response must have the same characteristics of steady state creep in sapphire single crystals as reported by Firestone and Heuer [3], albeit with certain important added complexities derived from the presence of the c-ZrO_2 phase. Figure 1 shows the well known phase morphology of a typical Al_2O_3/c-ZrO_2 eutectic where the bright phase is the c-ZrO_2. Very much like the γ' phase in superalloy single crystals of CMSX-3 [18], a

large fraction of the c-ZrO_2 has dimensions in the range of 0.2-0.4 μm and must be regarded as being too small to have the capability of undergoing plastic flow by independent internal processes of dislocation multiplication by glide or climb. The c-ZrO_2 phase components of larger dimensions (the irregular shaped ones in Fig. 1) should undergo rapid relaxation of shear stresses in the 1200-1520°C temperature range of interest, as the transient creep curve of Fig. 5 suggests. However, as the FEM analysis of Section 4.1 shows, complete shear stress relaxation in the c-ZrO_2 still leaves the mean normal stress intact in it which prevents large average stress enhancement in the Al_2O_3 phase.

Since the best slip systems of the basal and prismatic type are largely unstressed for glide due to the tight texture of the Al_2O_3 phase, and since the pyramidal dislocations of $1/3 < \bar{1}101 >$ type are sessile in glide, as discussed in Section 4.2, creep in this component for eutectic bars in tension, can only be a consequence of climb of the $(1/3) < \bar{1}101 >$ pyramidal edge dislocations. Nabarro [19] has presented an idealized model of creep derived entirely from climb of dislocations of a Frank-type network where material fluxes are between the actual climbing dislocations with Burgers vectors parallel to the stress axis and those of other types experiencing no climb forces. Firestone and Heuer [3] found reasonable agreement of their results with the Nabarro model where the stress exponents were in the range of 3 as that model predicts. In the case of the eutectics where the stress exponents are in the range of 4.5-6.0 different conditions should hold, requiring considerable modification of the Nabarro framework.

In our creep model it is assumed that the $(1/3) < \bar{1}101 >$ pyramidal dislocations pre-exist in the Al_2O_3 phase, and will multiply by well known topological convolution processes from Bardeen-Herring [20] sources, and will climb under stress during creep. The mean-free-path lengths of climbing dislocations in Al_2O_3 should involve several multiples of the interphase dimensions, requiring them to repeatedly bow and straighten-out as they thread through the small c-ZrO_2 domains that will remain impenetrable to them. Such repetition of transient line shapes can be viewed as the primary source of the elevation of the creep stress exponents to become larger than 3 [21]. The climb of these dislocations, will be diffusion controlled, provided that adequate jog concentrations are present along the dislocations. Such jogs are expected to be produced by nodal emission processes from network junctions rather than being of a thermal equilibrium nature which preliminary analyses show to be far too difficult. The diffusional material transport will be between dislocation cores and the large concentrations of incoherent or semi-coherent interfaces. These interfaces will be completely opaque to the transmission of dislocations from c-ZrO_2 to Al_2O_3 or vice versa. Residual stresses due to initial thermal misfit between the components will be relieved during the transient phases of the creep and provide another contribution to the recorded creep strain shown in Fig. 5, but that steady state creep will be governed by the climb forces resulting entirely from the applied stress.

5.2 The creep rate

Consider a round tensile creep bar of an Al_2O_3/c-ZrO_2 eutectic as sketched in Fig. 17 where local axes 1,2,3, are chosen in a pyramidal glide system with axis 1 parallel to the $1/3 < \bar{1}101 >$ Burgers vector, axis 2 normal to the pyramidal plane making an angle φ with the bar axis, and axis 3 parallel to the line vector of a positive edge dislocation. Under a uniform stress σ_1 a positive edge dislocation will climb in the negative 2 direction with a velocity v_c to contribute to a uniaxial tensile creep strain rate parallel to the 1 direction. This velocity, if it were governed by diffusion controlled climb would be given by [22]:

$$v_c = \frac{2\pi D(\sigma_1 - \sigma_T)b^2}{kTln(r_s/r_c)} \tag{2}$$

where $D = D_0 exp(-Q/RT)$ is the diffusion constant of Al_2O_3 where oxygen is recognized to be the slow diffusing species, σ_T is the triaxial component of the applied stress ($= \sigma_z/3$) that does not promote equilibrium climb, r_s is the distance from the dislocation core to vacancy sinks along the interfaces, r_c the core radius from which point defect emission is considered, b the magnitude of the Burgers vector, D_0 the pre-exponential factor of the diffusion constant, Q the activation energy of O ion diffusion in Al_2O_3 and R and T have their usual meaning. The kinematics of shape change due to climb alone of dislocations has been considered more broadly by Groves and Kelly [23]. In the case of the eutectics a more specialized consideration is adequate. Thus, considering that there will be three equivalent pyramidal systems that can contribute to the axial strain rate equally, the axial creep strain rate $\dot{\epsilon}_z$ along the bar and the accompanying radial contractile strain rates $\dot{\epsilon}_r$ are given respectively as [24]:

$$\dot{\epsilon}_z = (2 - 3cos^2\phi)\dot{\epsilon}_0 \tag{3a}$$

and

$$\dot{\epsilon}_r = -(1 - \frac{3}{2}cos^2\phi)\dot{\epsilon}_0 \tag{3b}$$

where

$$\dot{\epsilon}_0 = b\rho_m v_c \tag{4}$$

is the main creep rate in the pyramidal system coordinates without regard to overall volume preservation , which is considered to result in Eqns(3a) and (3b) [24]. Relating the actual climb-producing tensile stress σ_1 to the axial stress σ_z and considering the volume-average effect of the local variation of stress due to the presence of the c-ZrO_2 components by a factor q gives

$$\sigma_1 - \sigma_T = \frac{2}{3}q\sigma_z(1 - cos^2\phi) \tag{5}$$

If the mobile dislocation density, ρ_m, of climbing dislocations at steady state is governed by mutual interactions in a self adjusting basis [19]; i.e.

$$\rho_m \cong (\frac{2\pi\sigma_z}{\mu b})^2 q^2 (1 - cos^2\phi)^2 \tag{6}$$

one has, by finally combining Eqns (3a),(4),(5) and (6) the axial steady state creep rate:

$$\dot{\epsilon}_z = A(\frac{D}{b^2})(\frac{\sigma_z}{\mu})^3(\frac{\mu\Omega}{kT})\frac{(1 - cos^2\phi)^3(2 - 3cos^2\phi)}{ln(r_s/r_c)} \tag{7}$$

where

$$A = \frac{2}{3}(2\pi)^3\frac{q^3}{\beta} \tag{8a}$$

and

$$\beta = \Omega/b^3 = 0.079 \tag{8b}$$

where Ω is the ionic volume of O in the Al_2O_3 lattice and q is a factor which relates the local volume-average climb stress to the axial stress σ_z, as was determined from the FEM analysis of the stress distribution in the Al_2O_3 phase under an applied tensile stress, as presented in Section 4.1.

Eqn. (7) gives the creep rate due to the climb of quasi-straight dislocations in a homogeneous stress field. As is discussed in Section 5.3 this is not the case in the Al_2O_3/c-ZrO_2 eutectics where the climbing dislocations need to thread through the non-deforming c-ZrO_2 domains acting as dispersoids and are required to alternately bow around these domains and be released to straighten out, acting effectively as if straight dislocations were moving through a strongly varying internal stress field which will increase the stress exponent in predictable ways and decrease the actual creep rate [21].

In Section 5.4 the creep model is compared with the experimental results.

5.3 Effect of internal resistance variations

As stated in Section 5.2 the creep response of the Al_2O_3/c-ZrO_2 eutectics differ significantly from the creep behavior in homogeneous sapphire single crystals studied by Firestone and Heuer [3]. First because of the non-uniform stress distribution in the morphology of Al_2O_3 and c-ZrO_2 discussed in Section 4.1 above but even more importantly by the large perturbations that the climbing dislocations encounter threading through the isolated and largely non-deforming c-ZrO_2 domains. Thus, consider the convolutions that a climbing dislocation has to go through as it threads through the gaps of the c-ZrO_2 domains as depicted in Fig. 18. First, the climbing dislocation must squeeze into the gaps between the domains as depicted in Fig. 18a to a critical

configuration much like the Orowan bowing process for non-shearable dispersoids. The peak stress that is required for this configuration to be achieved is

$$\sigma = \sigma_i = \frac{2\mathcal{E}}{b\Lambda} = \frac{\mu b}{\Lambda} \tag{9}$$

where $\mathcal{E}$ is the dislocation line tension ($= \mu b^2/2$) and Λ is the size of the inter-domain gap. Clearly, here the process is not one of glide but climb where σ is the climb stress. Once the critical configuration is reached and the climbing dislocation surrounds the impenetrable domain and pinches off as shown in Fig. 18b, the separated dislocation has acquired a definite cusp where this shape of the dislocation will undergo accelerated climb due to the advantageous line tension effects. These required contortions of the dislocations are viewed as if they were the same as positive and negative internal stresses σ_i, retarding and then accelerating climb, very much like the corresponding cases of favorable and unfavorable internal shear stresses that a glide dislocation needs to go through between dispersoids. Such problems were treated in great detail by many investigators, but particularly thoroughly by Li [21], which illustrated that a gliding dislocation (in the present case a climbing dislocation) loses more time in the region of adverse internal stress than the time it gains in moving through regions of favorable internal stress. The effect is illustrated in Fig. 19 where 19a shows the sinusoidally varying internal stress σ_i and the prevailing climb stress σ. The most important consequence of such deceleration and acceleration of motion is an increase in the effective stress exponent m of the dislocation velocity, scaled by the ratio of σ_i/σ shown in Fig. 19b. A secondary effect is a factor $C = \bar{v}/v$ that gives the decrease in the average dislocation velocity relative to the velocity in unhindered climb shown in Fig. 19c, also scaled with the ratio of σ_i/σ. To assess a measure of the effect it must be noted from Fig. 1 that in much of the morphology the inter-domain distance Λ would appear to be between 0.3-1.0μm. Taking the small dimension to determine the maximum level of this effect, together with $b = 5.12 \times 10^{-10} m$ and $\mu = E/2(1+\nu) = 73GPa$ [17] at 1400°C we determine $\sigma_i = 125$MPa. For an applied stress $\sigma_z = 300$MPa, in the range of interest, that would give a volume-average climb stress $\sigma = q\sigma_z(1 - cos^2\phi)$ of 153MPa, and a ratio $\sigma_i/\sigma \approx 0.815$, Fig 19b indicates that the effective exponent of the stress in the velocity expression should increase to nearly $m = 3$ from unity as the maximum effect. Moreover, Fig. 19c gives $C = \bar{v}/v = 0.6$. Clearly, larger distances Λ should result in smaller effective internal stresses while smaller applied stresses should give increased ratios σ_i/σ. The overall net effect will be rather complex to assess. Here, it is considered that under the conditions described the net effect on the overall stress exponent of the creep rate will be to elevate it from $n = 3$ for the model presented above to $n = (m+2) = (2.5+2) = 4.5$ to $n = (3+2) = 5$. This consideration and the factor C, when incorporated into the creep model of smooth climb given by Eqn (7) will change it finally to

$$\dot{\epsilon} = AC(\frac{D}{b^2})(\frac{\sigma_z}{\mu})^n(\frac{\mu\Omega}{kT})\frac{(1 - cos^2\phi)^3(2 - 3cos^2\phi)}{ln(r_s/r_c)} \tag{10}$$

It is this expression that is compared with the experimental results in Section 5.4 below.

5.4 Evaluation of the creep model

The final creep model of Eqn(10) is evaluated now and compared with experimental results. In the comparison the expression is evaluated for both 1400°C and 1520°C. The following model parameters and material properties are used in the comparison:

$\mu = \frac{E}{2(1+\nu)} = 73$GPa at 1400°C and 63.4GPa at 1520°C [17]

$b = 5.12 \times 10^{-10}$m

$\Omega = 1.06 \times 10^{-29}$m^3

$q = 0.721$ as determined in Section 4.1

$\beta = \Omega/b^3 = 0.079$

$A = \frac{2}{3}(2\pi)^3(q^3/\beta) = 7.85 \times 10^2$

$\phi = 57.7^o$

$r_s = 0.5 - 2.0\mu$m, as estimated from micrographs (Fig. 7)

$r_c \approx b$

$D = 10^{-14}$cm^2/sec at 1400°C and 9×10^{-14}cm^2/sec at 1520°C determined from Oishi and Kingery directly for their polycrystalline material [25] for which, parenthetically the activation energy was Q=110kcal/mol, considerably larger than our value.

Finally, we take $n = 4.5$ as suggested from the analysis in Section 5.3 above, and

$C = 0.6$.

The calculated steady state creep rate relations for 1400°C and 1520°C are presented in Fig. 6 as the broken lines in comparison with the experimental data.

Considering the several uncertainties in the model and material parameters the agreement between model and experimental results is very good.

6 Discussion

The experimental measurements of steady state creep rates in the Al_2O_3/c-ZrO_2 eutectic, while few, have given a good measure of the response of this material in the temperature range of interest. Taking account of the possible interactions of the c-ZrO_2 phase with the Al_2O_3 we have developed a steady state creep model based on climb of pyramidal edge dislocations in Al_2O_3 alone. In the model it is proposed that the c-ZrO_2 phase of relatively large size, in the micron range will most likely undergo nearly complete stress relaxation in the 1400°C range, resulting in an initial transient creep with relatively short time constant of roughly 200 seconds [2]. On the other hand the sub-micron size domains of the c-ZrO_2 will most likely be too small to undergo independent deformation processes by crystal plasticity and will remain non-deformable to impede the climb motion of the pyramidal system dislocations in the

Al_2O_3 much like dispersoids. The observed creep rate stress exponents in the range of 4-5 are indicative of this behavior. In this sense it would appear that the eutectic through its unique morphology should be more creep resistant than sapphire of [0001] axis orientation. To explore this comparison the creep model is re-interpreted for application to sapphire in which the climb motion of the dislocations is expected to be quasi-smooth. Such a modification would give a steady state creep expression of

$$\dot{\epsilon}_{sap} = A'(\frac{D'}{b^2})(\frac{\sigma_z}{\mu})^3(\frac{\mu\Omega}{kT})\frac{(1-cos^2\phi)^3(2-3cos^2\phi)}{ln(r_s/r_c)} \tag{11}$$

where $A' = \frac{2}{3}(2\pi)^3/\beta = 2.09 \times 10^3$ (for q=1.0)
and D', the diffusion constant, must be chosen for sapphire single crystals not having the benefit of diffusion short circuits along interfaces. From Oishi and Kingery [25] we obtain $D' = 3.5 \times 10^{-17}$cm^2/sec at 1400°C, or a factor of 3.5×10^{-3} lower than for polycrystalline material or for the eutectic with a large volume concentration of interfaces. For these alterations, but for all other factors remaining the same a steady state creep expression can be determined for sapphire crystals of [0001] orientation at 1400°C which is shown as the dashed line in Fig. 6, confirming the expectation of a lower creep resistance in comparison with the Al_2O_3/c-ZrO_2 eutectic.

The creep model that was presented is based on the existing evidence of the measured creep rates, their stress and temperature dependence and on the findings of the earlier work of Firestone and Heuer [3] on single crystal sapphire. However, the work leaves many unanswered questions. Foremost among these are the details of the continuance of the all-important fluxes of climbing dislocations, their origins, their form of maintenance and the fine structure of cores of dislocations such as details of jogs where the actual climb steps occur by O ion vacancy emission. Preliminary energetic considerations of dislocation emission from ledges on the ubiquitous interfaces or from misfit dislocations along interfaces have indicated very large energy barriers under the prevailing local stresses. However, other forms of heterogeneous nucleation of dislocations from interfaces must still be considered. Other possibilities for inelastic behavior such as Coble creep were discounted because of the apparent general absence of transverse boundaries in the topologically continuous Al_2O_3 component and the generally linear stress dependence of creep flow by this mechanism, which if present, appears to be swamped by dislocation climb flow. Some of these possible mechanisms as well as the missing details of the maintenance of climb fluxes could come from TEM studies which were in progress at the preparation of this final report.

7 Conclusions

1. In the eutectic of Al_2O_3/c-$ZrO_2(Y_2O_3)$ the majority phase of Al_2O_3 is topologically continuous, has a nearly perfect texture of [0001] parallel to the growth direction and en-

capsulates everywhere the minority c-ZrO_2 phase which itself has a growth texture of $< 112 >$.

2. The interfaces separating the phases are well structured but are incoherent over most of the area.

3. A large fraction of the c-ZrO_2 phase has a sub-micron oriented fibrillar or plate-like morphology which often, but not always, aggregates into colonies. The remaining fraction, usually surrounding the colonies of oriented fibrils or platelets is of a coarser, micron size.

4. Upon first application of stress, transient creep is observed which is attributed to stress relaxation in the coarser fraction of the c-ZrO_2. The sub-micron fraction is considered to be too small to undergo deformation by crystal plasticity and is expected to be dormant.

5. In steady state creep, stress changes do not produce additional transients within the resolution of stress measurements.

6. The stress dependence of steady state creep rate is of power-law form with an exponent in the range between 4.5 to 5.0. The activation energy of the creep rate is 71.1 kcal/mol in the 1200-1520°C range and is attributed to oxygen ion diffusion through the Al_2O_3 and along the interfaces.

7. Because of the [0001] texture of the Al_2O_3 phase which must control the overall creep rate for topological reasons, the proposed steady state model is based on the climb of the $(1/3) < \bar{1}101 >$ pyramidal dislocations in Al_2O_3 since the latter are sessile in glide.

8. In the creep model which is a generallization of the steady state diffusional creep model of Nabarro [19], the stress exponents of larger than 3 are attributed to the necessity of repeated bowing and straightening of the climbing dislocations in Al_2O_3 as they circumvent the sub-micron c-ZrO_2 domains.

9. The predictions of the creep model, which has no adjustable constants, agree quite well with experimental observations.

10. Finally, a mechanistic comparison of the creep resistance of the Al_2O_3/c-$ZrO_2(Y_2O_3)$ eutectic with that of [0001] sapphire single crystal indicates that the former appears superior because of the obstructions of the dispersoid-like c-ZrO_2 domains to the the climbing dislocations of the Al_2O_3 phase, even though the diffusion constant of sapphire single crystals is three orders of magnitude smaller than that of the eutectic.

References

[1] Fleischer, R.L., *J. Mater. Sci.*, 1987, **22**, 2281

[2] Sayir, A. and Farmer, S. C., *Acta Mater.* , 2000, **48**, 4691

[3] Firestone, R.F. and Heuer, A.H., *J. Amer. Ceram. Soc.* , 1976, **59**, 24

[4] Chiang, J., Bodur, C.T. and Argon, A.S., *Phil. Mag. Letters* , in the press.

[5] Bodur, C.T., Chiang, J. and Argon, A.S., submitted to the *J. European Ceram. Soc.*

[6] Edelin, G. and Poirier, J.P., (in French) *Phil. Mag.* , 1973, **28**, 1203

[7] Morgan, P.-E.-D. and Marshall, D.B., *J. Amer. Ceram. Soc.* , 1995, **78**, 1553

[8] Lev, L.C. and Argon, A.S., *Mater. Sci.&Engrg.* , 1995, **A195**, 251

[9] Sayir, A., unpublished report: NASA Glenn Research Center, private communication.

[10] Fraser, C.S., Dickey, E.C. and Sayir, A., *J. Cryst. Growth* , 2001, **233**, 187

[11] Yi, J. and Argon A.S., to be published.

[12] Pastor, J.Y. Poza, P., Llorca, J., Pena, J.I., Merino, R.I. and Orera, V.M., *Mater. Sci. & Engrg.* 2001, **A308**, 241

[13] Mazerolles, L., Michol, D. and Portier, R., *J. Amer. Ceram. Soc.* , 1986, **69**, 252

[14] Haubensak, F. and Argon, A. S., *J. Mater. Sci.* , 1997, 32, 1473

[15] Messerschmidt, U., Baufeld, B. and Baither, D., *Key-Engineering Materials* , 1998, **153-154**, 143

[16] Argon, A.S., Yi, J. and Sayir, A., *Mater. Sci. Engrg.* , 2001, **A319-321**, 838

[17] Wolfenden, A., *J. Mater. Sci.* , 1997, **32**, 2275

[18] Pollock, T.M. and Argon, A.S., *Acta Metall.* , 1992, **40**, 1

[19] Nabarro, F.R.N., *Phil. Mag.* , 1967, **16**, 231

[20] Bardeen, J. and Herring, C., In: "Imperfections in Nearly Perfect Crystals", edited by Shockley, W., Hollomon, J.H., Maurer, R. and Seitz, F., J. Wiley & Sons, NY, pp.261-288, 1952

[21] Li, J.C.M., In: "Dislocation Dynamics", edited by Rosenfield, A.R., Hahn, G.T., Bement, Jr. A.L. and Jaffee, R.I., McGraw-Hill: New York pp.87-116, 1968

[22] Friedel, J., in "Dislocations", Addison-Wesley, Reading, MA, p. 104, 1964

[23] Groves, G.W. and Kelly, A., *Phil. Mag.* , 1969, **19**, 977.

[24] Yi, J., Argon, A. S. and Sayir A., submitted to the *J. European Ceramic Soc.*

[25] Oishi, Y. and Kingery, W.D., *J. Chem. Phys.* , 1960, **33**, 480.

[26] Refson, K., MOLDY: "A portable molecular dynamics simulation program for serial and parallel computation", *Comput. Phys. Commun.* , 2000, **126** , 310

[27] Kronberg, M. L., *Acta Metall.* , 1957, **5**, 507

[28] Dickey, E.C., Frazer, C.S., Watkins, T.R. and Hubbard, C.R., *J. European Ceram. Soc.* , 1999, **19**, (Nos 13-14), 2503-2509

Table 1: Recorded Steady State Strain Rates

Stress (MPa)	Strain Rate $\dot{\epsilon}$(sample #)[$\dot{\bar{\epsilon}}$ average rate] (sec^{-1})
1200°C	
200	1.97×10^{-10} (142-18)
1400°C	
200	3.6×10^{-9} (187-29)
225	2.26×10^{-9} (187-27-2); 8.16×10^{-9} (187-27-1) [5.21×10^{-9}]
250	5.53×10^{-9} (187-29)
275	9.95×10^{-9} (187-27-2); 1.10×10^{-8} (187-27-1) [1.048×10^{-8}]
1520°C	
150	1.57×10^{-9} (142-16); 4.40×10^{-9} (142-16) [2.98×10^{-9}]
200	1.20×10^{-8} (142-16); 1.60×10^{-8} (142-16) [1.40×10^{-8}]

Table 2: Material Properties for Linear Elastic FEM Analysis

	Al_2O_3	c-ZrO_2
Young's Modulus	190GPa at 1400°C	0.05MPa at 1400°C [a]
Poisson's ratio	0.3	0.4999999 [a]
Yield Stress	5.0GPa [b]	5.0GPa
Coefficient of Thermal Expansion, $°C^{-1}$	9.1×10^{-6} (a) 9.9×10^{-6} (c)[28]	$12.9\cdot10^{-6}$ [28]

[a] These valurs were chosen in the FEM code result in a negligible shear modulus of 83GPa for c-ZrO_2 to obtain a state of near complete shear relaxation while leaving the bulk behavior intact.

[b] These high yield stresses were chosen in the FEM code to guarantee pure elastic response.

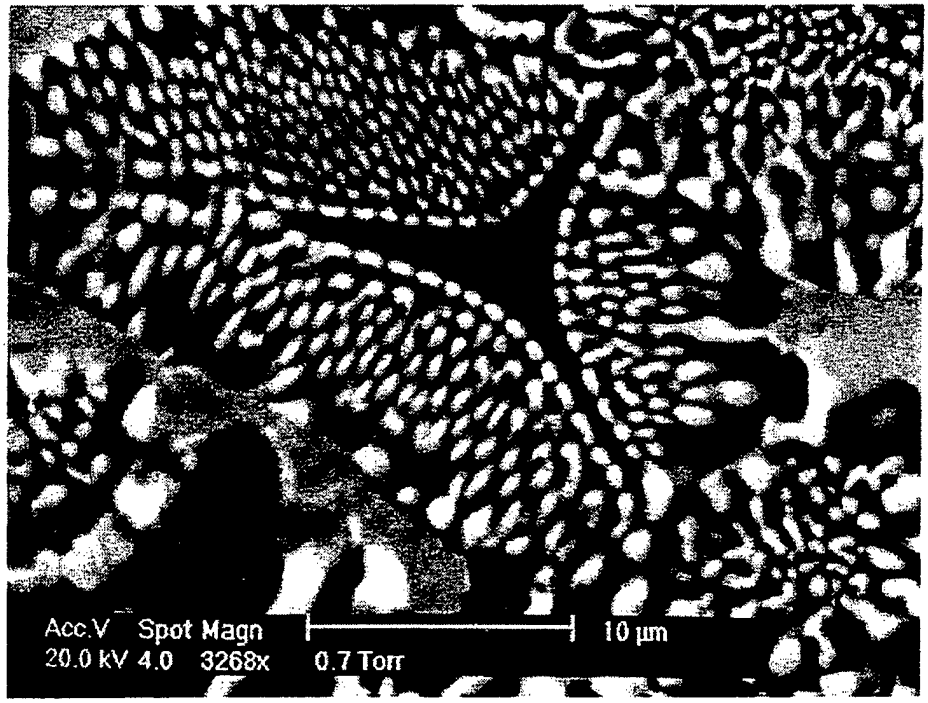

Figure 1: An SEM micrograph of a typical morphology of the Al_2O_3/c-ZrO_2 eutectic, as revealed in a transverse section. The black component is Al_2O_3. Much of the c-ZrO_2 component (the bright regions) is of low sub-micron size and is expected not to deform by any form of crystal plasticity.

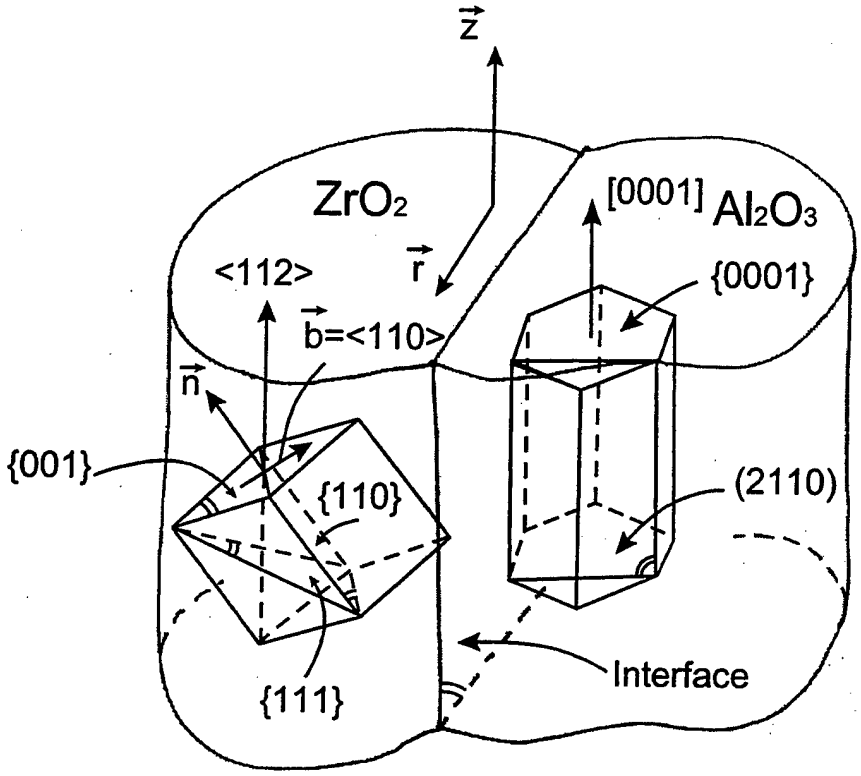

Figure 2: Sketch showing the textural arrangement of the Al_2O_3 component with a preferred [0001] axis and c-ZrO_2 with a preferred $< 112 >$ axis found by electron diffraction analysis. Other textures for c-ZrO_2 have also been reported.

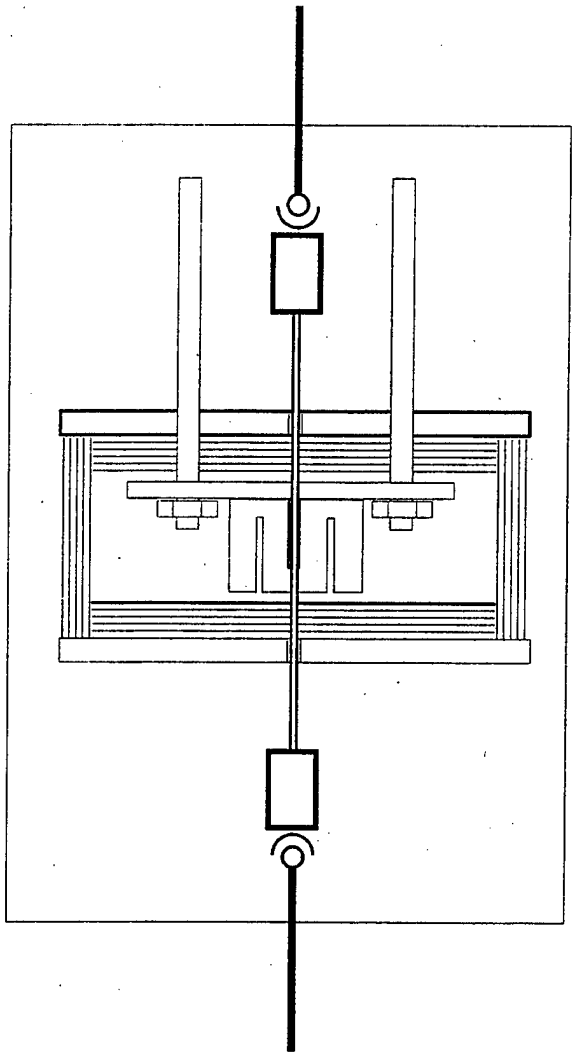

Figure 3: A cut-out view of the hot zone of the high temperature chamber for creep experiments showing also the cold grips of specimens, and the water cooled Cu baffles between the hot zone and the grips.

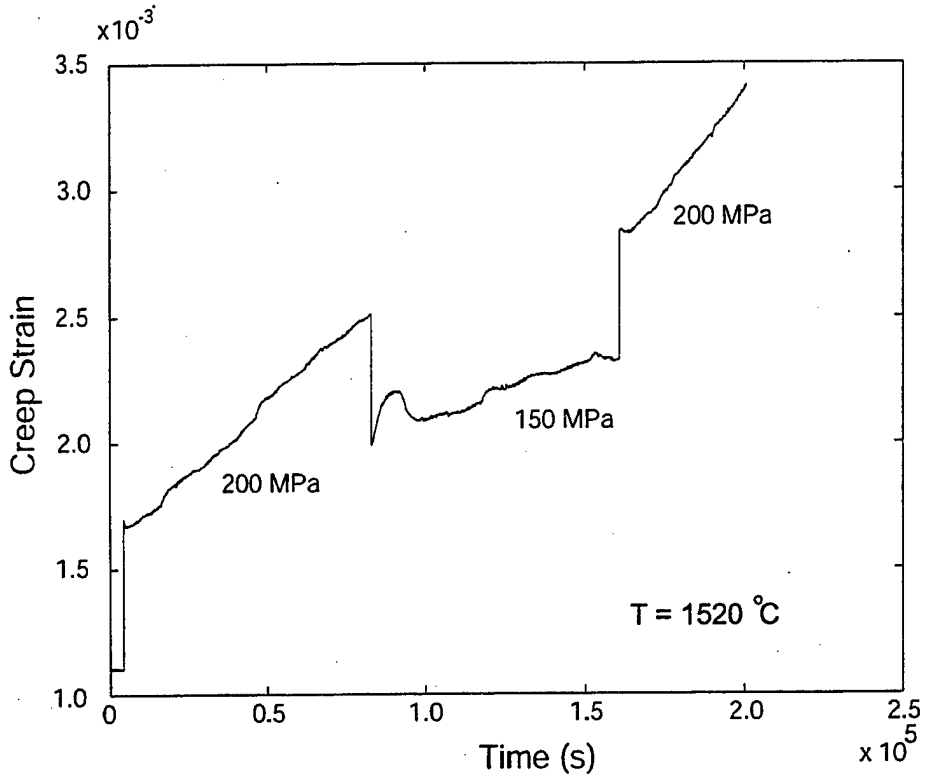

Figure 4: A typical strain time plot for steady state creep at two different stress levels in an Al_2O_3/c-ZrO_2 eutectic rod at 1520°C

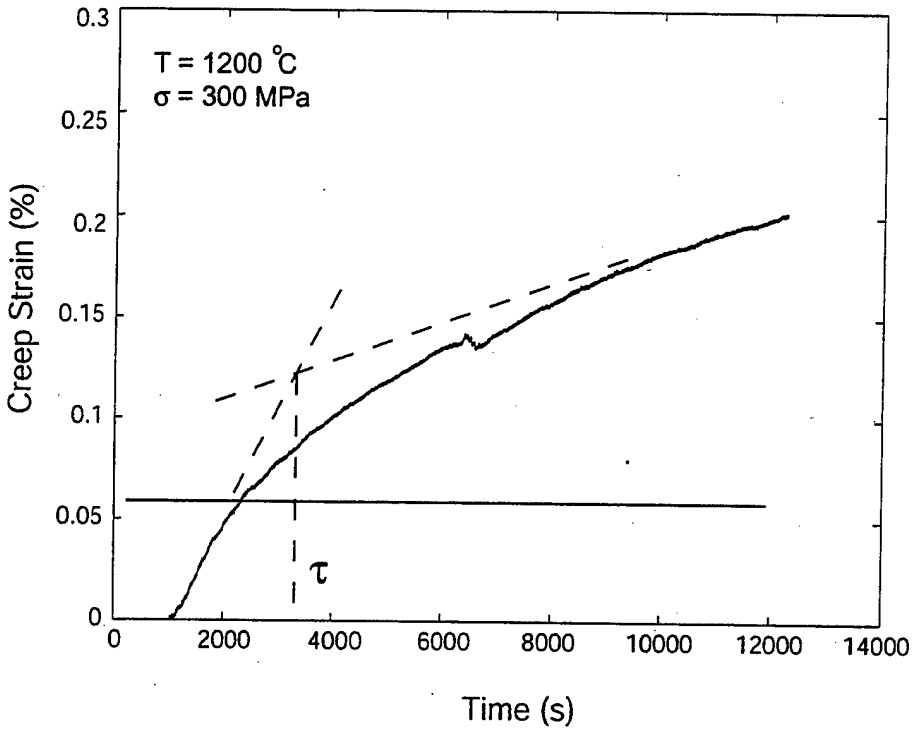

Figure 5: A typical creep strain transient in an Al_2O_3/c-ZrO_2 eutectic under a stress of 200 MPa at a temperature of 1200°C. The horizontal line gives an estimate of creep strain increment due to stress relaxation in the coarse fraction of c-ZrO_2.

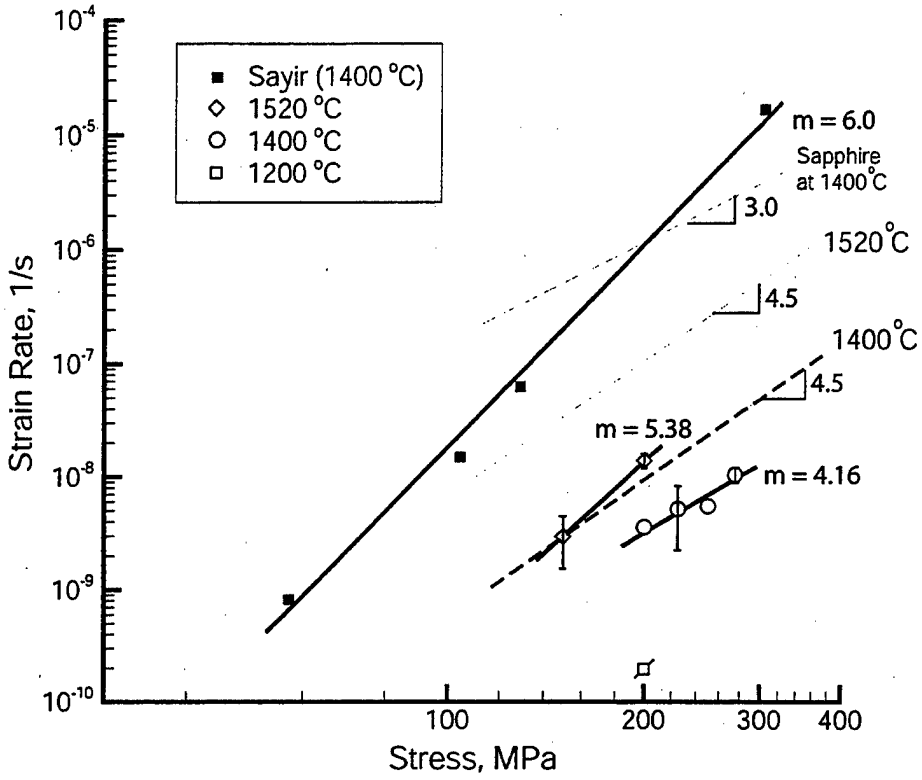

Figure 6: Plots of steady state creep rates as a function of stress for temperatures of 1200, 1400 and 1520°C compared with measurements reported by Sayir and Farmer [2]. Broken lines represent predictions of creep model for Al_2O_3/c-ZrO_2 at 1400°C and 1520°C, together with model prediction for sapphire at 1400°C

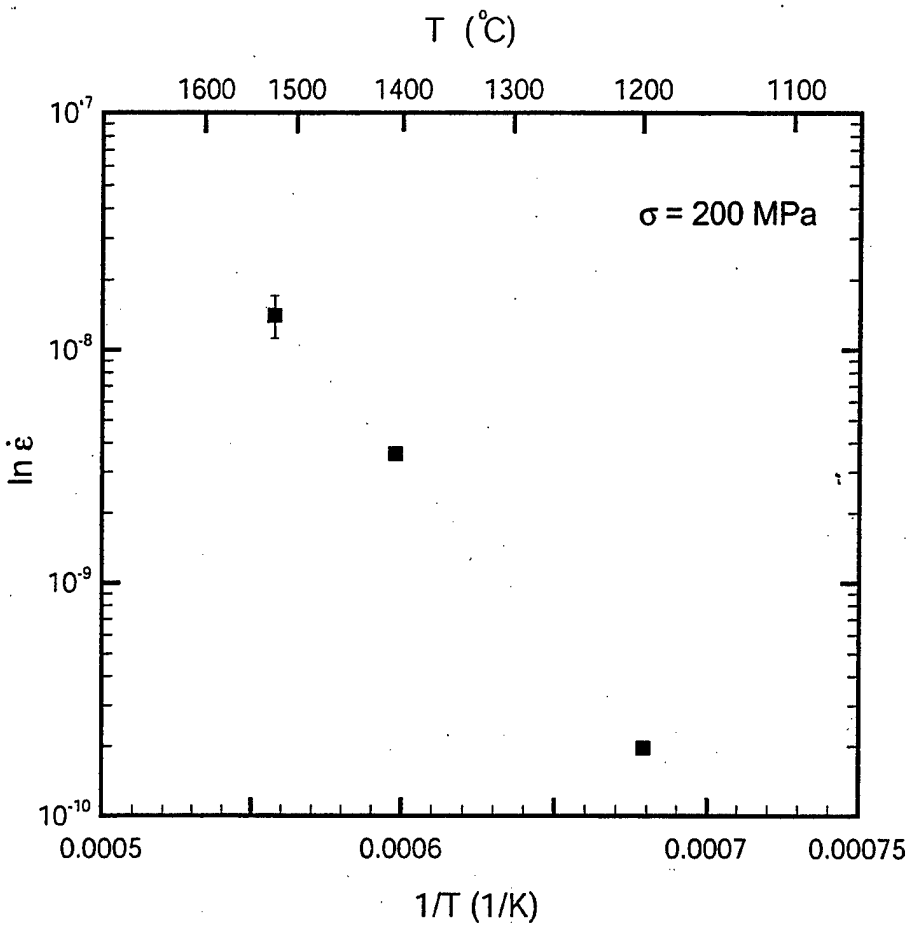

Figure 7: Determination of activation energy of steady state creep from temperature dependence of steady state creep rate.

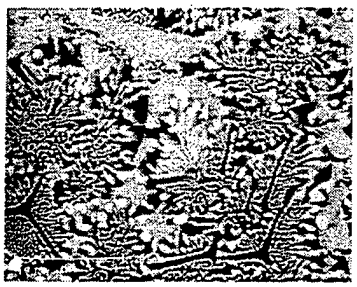

(a)

(b)

Figure 8: A Vickers indentation (a), and one of the cracks extending from one corner of the indentation (b). The crack contour is used to estimate the fracture toughness of the eutectic.

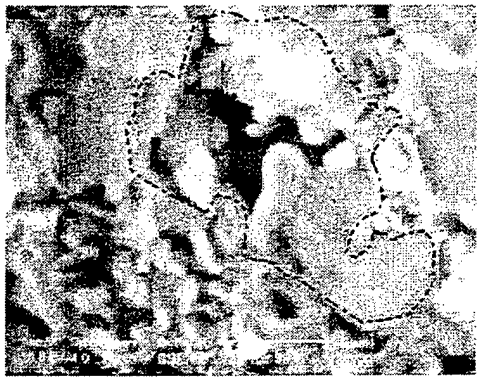

(a)

(b)

Figure 9: An internal pore (a), and a surface flaw (b), observed on the premature fractured surface of a sample. The size and shape of these defects are used to estimate the fracture toughness of the eutectic

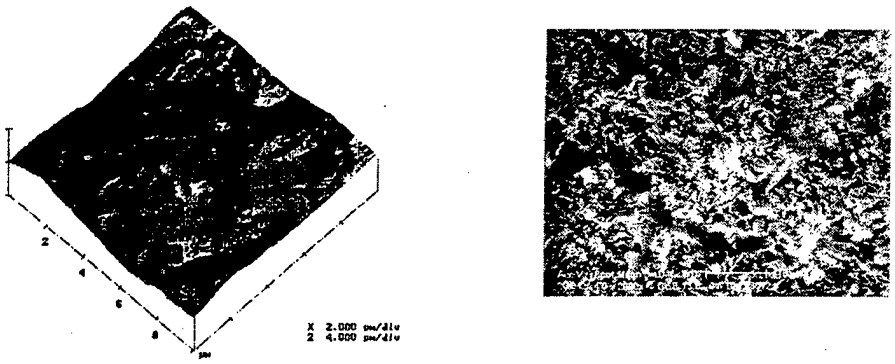

Figure 10: An AFM fracture surface profile characterization (a), and corresponding SEM picture (b).

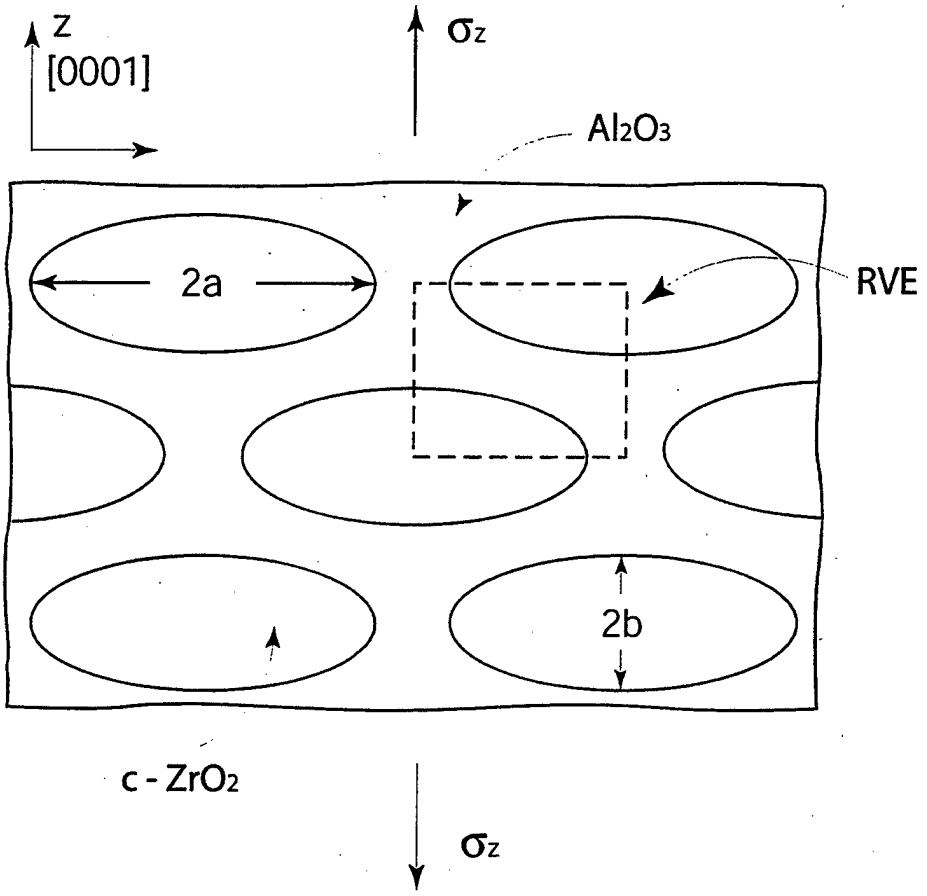

Figure 11: Sketches of an idealization of the c-ZrO_2 domains as ellipsoidal cylinders in the topologically continuous Al_2O_3 component, for the purpose of a FEM study of the internal stress distribution in the Al_2O_3 when a tensile stress σ_z is applied.

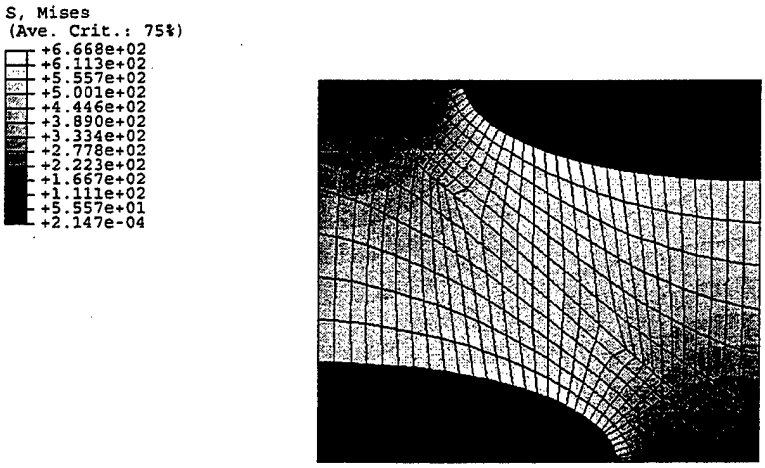

(a)

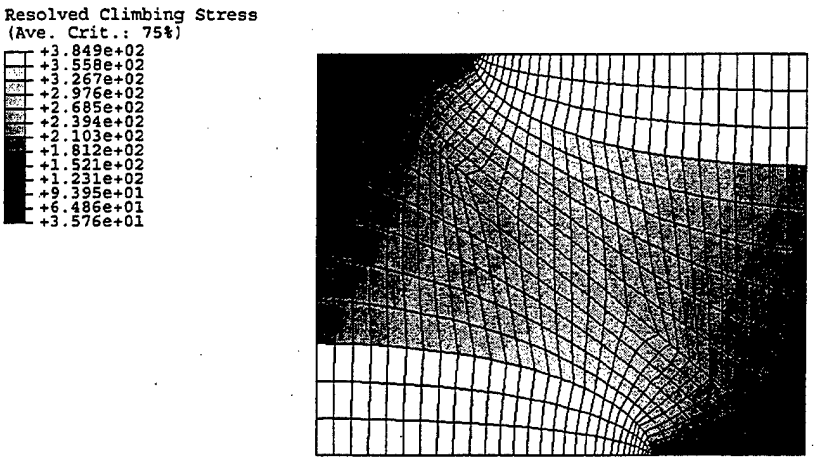

(b)

Figure 12: Stress distribution results of the FEM study; a) deviatoric (Mises) stresses in the two components of the eutectic; b) the distribution of the climb stress σ_1 in the Al_2O_3.

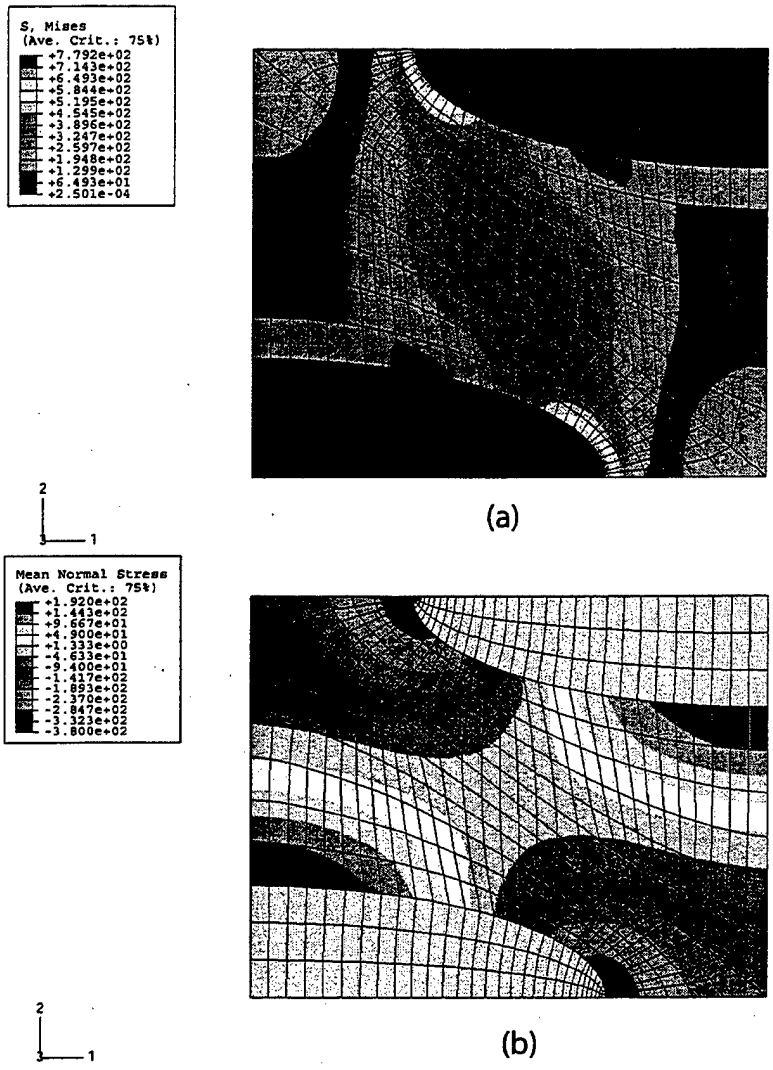

Figure 13: The deviatoric von Mises stresses, (a); and the mean normal stresses, (b) of a temperature reduction from 1875°C to 1400°C

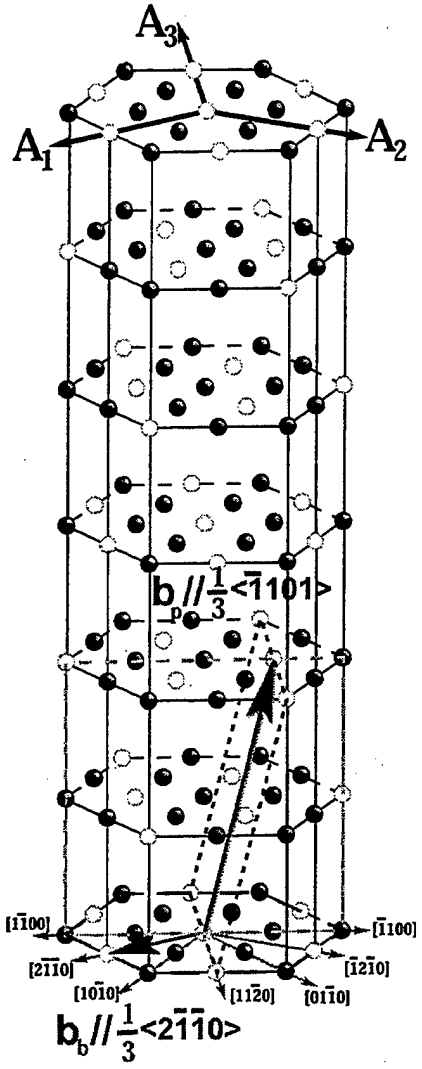

Figure 14: The cation sub-lattice of sapphire showing the three prominent slip system in the basal plane; in the prism planes(broken lines); and the pyramidal planes (dashed) lines.

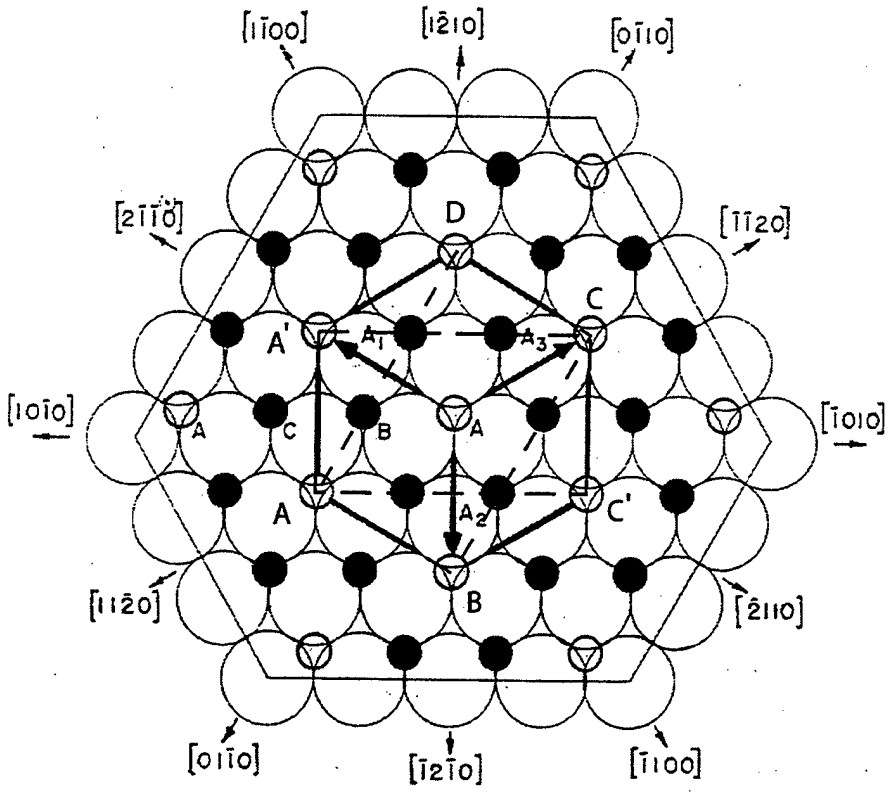

Figure 15: The idealized arrangement of ions viewing the base plane from above [000$\bar{1}$]. The large open circles represent an underlying layer of oxygen anions; the empty interstial sites are occupied by the oxygen anion layer immediately above; the small filled circles represent aluminum cations (in the real crystal these do not lie in a single plane but are alternately associated closer to one or the other nearest oxygen layers where they produce in-plane distortions); the empty small circles represent aluminum holes which specify the scale of prefect dislocation Burgers vectors. The reference rectangle ABCD represents the base plane of the simulation cell for the base plane edge dislocation, while the rectangle AA'CC' represents a symmetry plane in the simulation cell for the pyramidal edge dislocation (after Kronberg 1957).

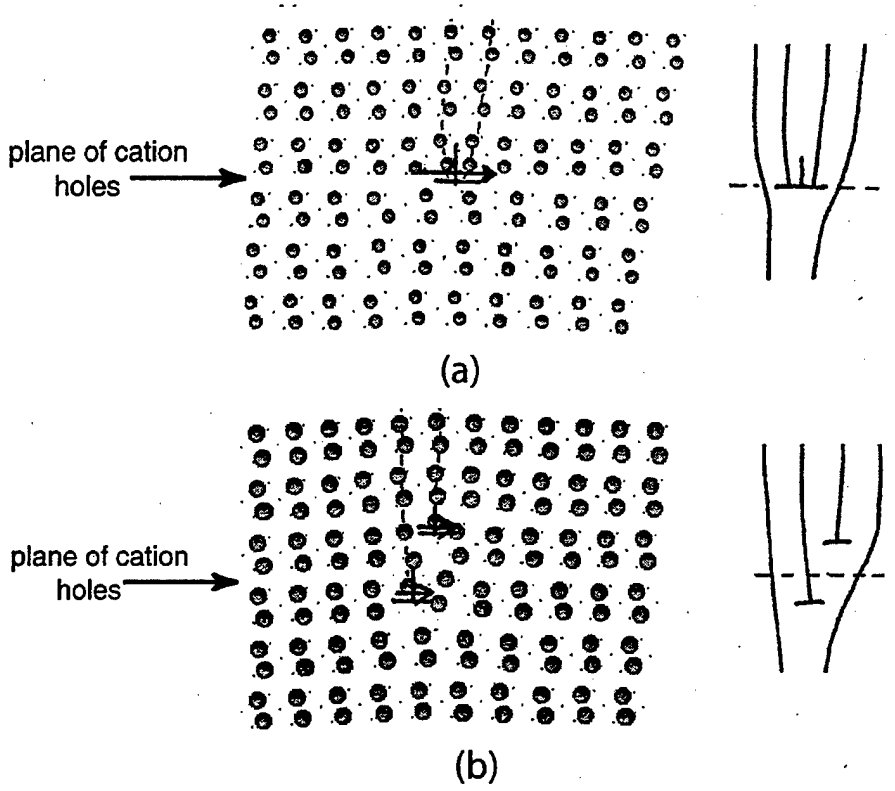

Figure 16: Pyramidal plane edge dislocations viewed in the Al_2O_3 structure from the $[11\bar{2}0]$ direction. Dislocations are on $(1\bar{1}02)$ planes with $b = 1/3 < \bar{1}101 >$, a)Unrelaxed dislocation viewed in the cation (Al) lattice has high energy but could glide on cation "hole" plane; b) relaxed dislocation of lower energy splits core into two fractional edge dislocations lying on parallel cation planes of very high resistance making dislocation immobile.

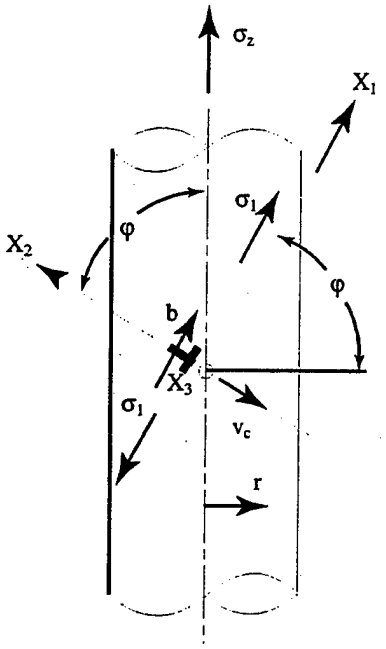

Figure 17: Sketch of a round bar of a Al_2O_3/c-ZrO_2 eutectic with z axis parallel to the [0001] direction of the Al_2O_3. The plane at angle ϕ outlines a pyramidal glide plane. A local tensile stress σ_1 will make a positive edge dislocation climb in the negative X_2 direction.

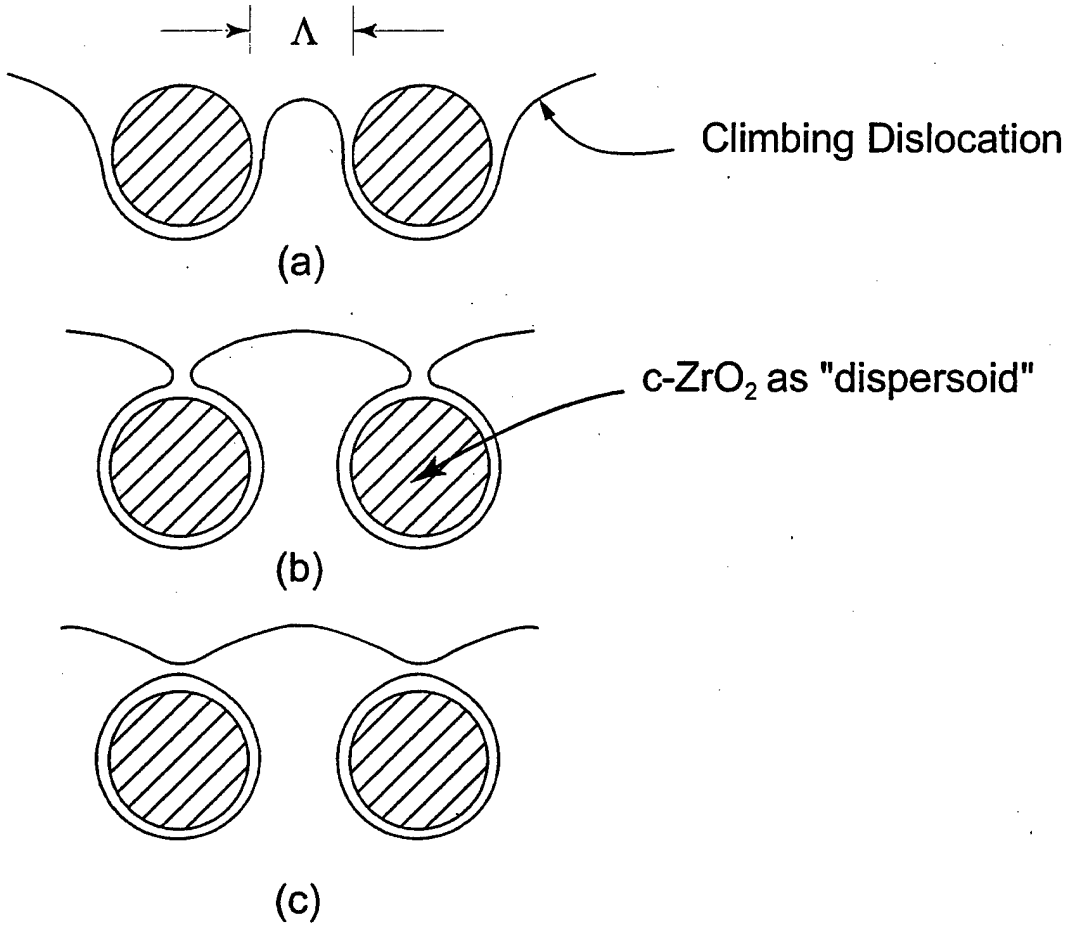

Figure 18: Sketch depicting the required contortions that a climbing edge dislocation needs to suffer in bowing through the gaps between the c-ZrO_2 domains that we consider to be impenetrable: a) critical climb configuration to bow through the gap between two c-ZrO_2 dispersoids at a spacing Λ; b) at the point when the climbing dislocation is just about to pinch off; c) the cusped dislocation line straightening out under the application of line tension.

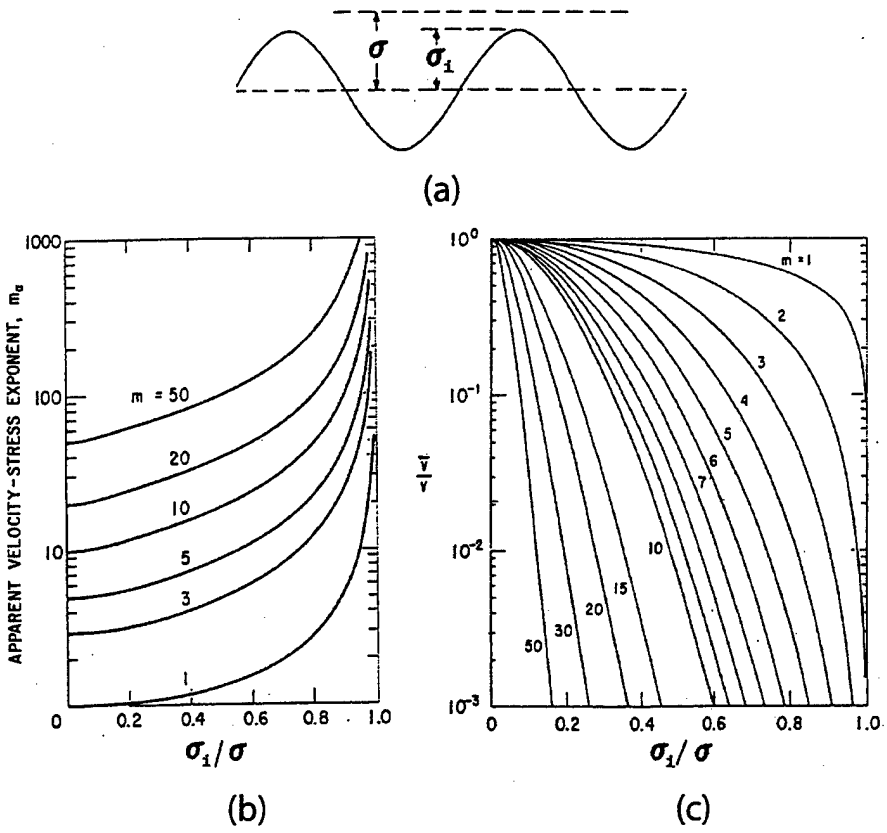

Figure 19: Consequence of the repeated bowing out and straightening of the climbing dislocation considered as a set of internal resistance σ_i alternately retarding and speeding up the climbing dislocation: a) retardation and speeding up considered as unfavorable and favorable internal stresses σ_i in the presence of a climb stress σ; b) effect of σ_i/σ on the overall stress exponent m of the dislocation velocity; c) effect of σ_i/σ on the attenuation factor C on the average climb velocity. (figures reproduced from Li [20], courtesy of J. Wiley & Sons)

Appendix

A Personnel taking part in the program

A. S. Argon, Principal investigator/Program director, Professor of Mechanical Engineering, M.I.T.

J. Yi, Research assistant, Mechanical Engineering, M.I.T., Candidate for the Ph.D. degree. (2/1/99-present)

C.T. Bodur, Visiting Scientist, Mechanical Engineering, M.I.T., on leave from the Technical University of Istanbl, Turkey, NATO/TUBITAK Fellow. (9/1/02-2/28/03).

J.P. Chang, Graduate Student, Nuclear Engineering, M.I.T. (1/15/03-3/15/03).

B External collaborations

A. Sayir, Principal Collaborator, Senior Research Scientist, Materials Division, NASA John Glenn Research Center, Cleveland, OH.

E. C. Dickey, Assoc. Prof., Materials Science & Engineering, Penn State University, University Park, PA.

C Presentations

A. S. Argon, J. Yi and A. Sayir, "Creep Resistance of Directionally Solidified Ceramic Eutectics of Al_2O_3/c-ZrO_2 with Sub-micron Columnar Morphologies", presented at the "12th International Conference on the Strength of Materials" held at Ailomar Coference Site, CA on 8/27/2000.

A. S. Argon, E. C. Dickey and A. Sayir, "Creep Resistance of Directionally Solidified Ceramic Eutectic," presented at the TMS/ASM Symposium on "Rate Processes in Plastic Deformation II: Towards a Unified Theory of Deformation - II. held at St. Louis, MO, 10/9-12/2000.

A. S. Argon, J. Yi and A. Sayir, "Creep Resistance of the Directionally Solidified Ceramic Eutectic of Al_2O_3/c-ZrO_2: Experiments and Models", presented at the "Directionally Solidifed Ceramics Workshop" at Ecole des Mies, in Paris, France on 5/5/2003

C. T. Bodur, J. Chang and A. S. Argon, "Molecular Dynamics Simulations of Basal and Pyramidal System Edge Dislocations in Sapphire and their Role in Creep of Ceramic Eutectics", presented at the "Directionally Solidified Ceramics Workshop" at Ecole des Mies in Paris, France on 5/7/2003

D Publications

A. S. Argon, J. Yi and A. Sayir, "Creep resistance of directionally solidified ceramic eutectics of Al_2O_3/c-ZrO_2 with sub-micron morphologies", Mater. Sci. Eng. A319-321, 838(2001)

J. Chang, C. T. Bodur and A. S. Argon, "Pyramidal edge dislocation cores in Sapphire", Phil. Mag. Letters, in the press.

J. Yi, A. S. Argon and A. Sayir, "Creep resistance of the directionally solidified ceramic eutectic of Al_2O_3/c-ZrO_2(Y_2O_3): Experiments and Models", under review in the J. European Ceramic Society.

C. T. Bodur, J. Chang and A. S. Argon, "Molecular dynamics simulations of basal and pyramidal system edge dislocation cores in Sapphire and their role in creep of ceramic eutecitcs", under review in the J. European Ceramics Society.